Local Mode Analysis of 2D ICRF Wave Solutions*

D. A. D'Ippolito and J. R. Myra

Lodestar Research Corporation,
Boulder, Colorado

E. F. Jaeger, L. A. Berry, and D. B. Batchelor

Oak Ridge National Laboratory,
Oak Ridge, Tennessee

*Work supported by US DOE Grants/Contracts DE-FC02-01ER54650, DE-FG03-97ER54392, and DE-AC05-00OR22725

Presented at the 44th APS-DPP Meeting,
Orlando, Florida, November 11-15, 2002

Abstract Submitted for the Forty-Fourth Annual Meeting

Division of Plasma Physics

November 11 – 15, 2002

Category Number and Subject:

5.3.0, Heating and Current Drive; Theory Poster

Local Mode Analysis of 2D ICRF Wave Solutions[1] D.A. D'Ippolito, J.R. Myra, *Lodestar Research Corp.*, E.F. Jaeger, L.A. Berry, D.B. Batchelor *ORNL* – Motivated by the growing capability of numerical rf simulations,[2] there is a critical need to develop appropriate post-processing tools for extracting physical information from the numerical solutions. Full-wave ICRF codes yield complicated rf field patterns, and the challenge is to understand these patterns by appealing to the intuitive, but approximate, physics-based notion of local plasma modes (global eigenmodes, transmitted and reflected waves, and mode conversions between different types of waves). Quantitative information on the local wavevectors, amplitudes and wave polarizations is desired, both for basic understanding and for use in calculating the ICRF-driven flows[3]. Here, progress will be reported on developing numerical techniques (windowed Fourier transforms and wavelets) for the local mode analysis of 2D toroidal ICRF field solutions[2], including mode-conversion scenarios, as part of the rf SciDAC project.

1. Work supported by US DOE grants DE-FC02-01ER54650, DE-FG03-97ER54392 and contract DE-AC05-00OR22725.

2. E.F. Jaeger, L.A. Berry, et al., Phys. Plasmas **9**, 1873 (2002).

3. J.R. Myra, D.A. D'Ippolito, E.F. Jaeger, L.A. Berry, D.B. Batchelor, this conference.

Introduction

● New post-processing tools are needed to extract important physical information from numerical simulations relevant to fusion (e.g. turbulence and rf wave codes). We are particularly interested in general techniques that may be useful in more than one area.

● Here, we consider an rf application. Full-wave ICRF codes yield complicated rf field patterns which we would like to understand in terms of *local plasma modes*:

- global eigenmodes
- transmitted and reflected waves
- mode conversion between different types of waves

● The output of such an analysis should be information on the local wavevectors **k**(**x**), wave amplitudes and wave polarizations for comparison with analytic theory and for use in subsequent post-processing calculations.

● We have compared several numerical techniques based on Fourier and wavelet transform methods. These methods are applied to a DIII-D D(H) fast wave-IBW mode-conversion case computed by the 1D AORSA full-wave code. The advantages and disadvantages of each technique will be described.

This work is partly funded by the rf SciDAC project.

Fourier Transforms

Given $f_i = f(x_i)$ compute the 1D transforms $f(x_i) \leftrightarrow F(k \equiv k_n)$, for i, n = 1 to N, where $k_n = -k_{max} + (n-1)\,\Delta k$, $\Delta k = \pi/L$ and $k_{max} = \pi/\Delta$ are the min and max k's, $2L = x_{N+1} - x_1$ = periodicity length, and $\Delta = x_2 - x_1$ = grid spacing.

• Fast Fourier Transform (FFT)

$$F_n = \frac{1}{N}\sum_{i=1}^{N} f_i \exp[-(i\,k_n x_i)] \quad , \qquad (1)$$

$$f_i = \sum_{n=1}^{N} F_n \exp[i\,k_n x_i] \quad . \qquad (2)$$

- global k's (no spatial information); not adequate for mode identification.

• Windowed Fourier Transform (WFT)

$$F_n(x_0, x_w, k_n) = \frac{1}{N}\sum_{i=1}^{N} f_i \exp[-(i\,k_n x_i)] \exp\left[-\frac{(x_i - x_0)^2}{2\,x_w{}^2}\right] \quad , \qquad (3)$$

- 2 parameters: window position x_0 and width x_w
- For constant x_w, $F_n = F_n(x_0, k_n)$
- A constant window width cannot simultaneously resolve long and short wavelength waves (see Fig. 1)

Fig. 1(a) x_W = 0.25 m

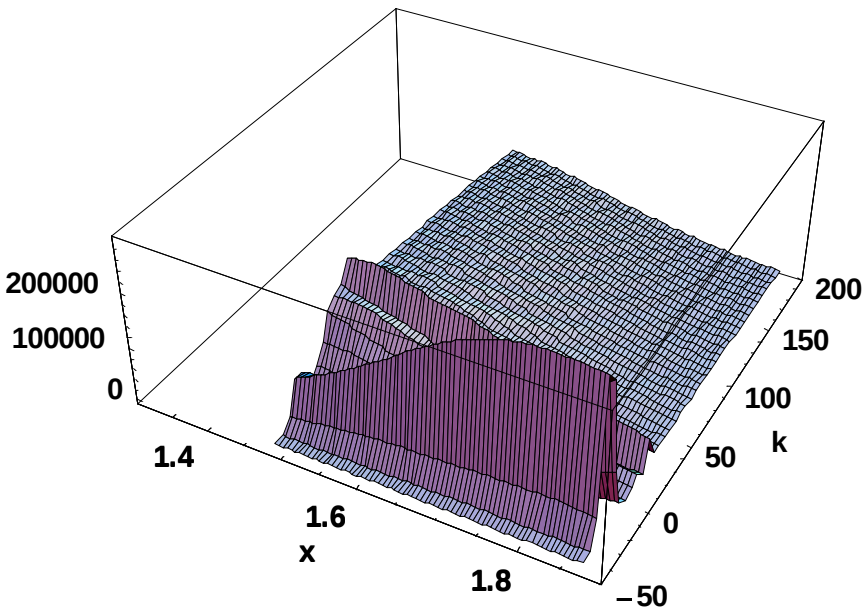

Fig. 1(b) xw = 0.05 m

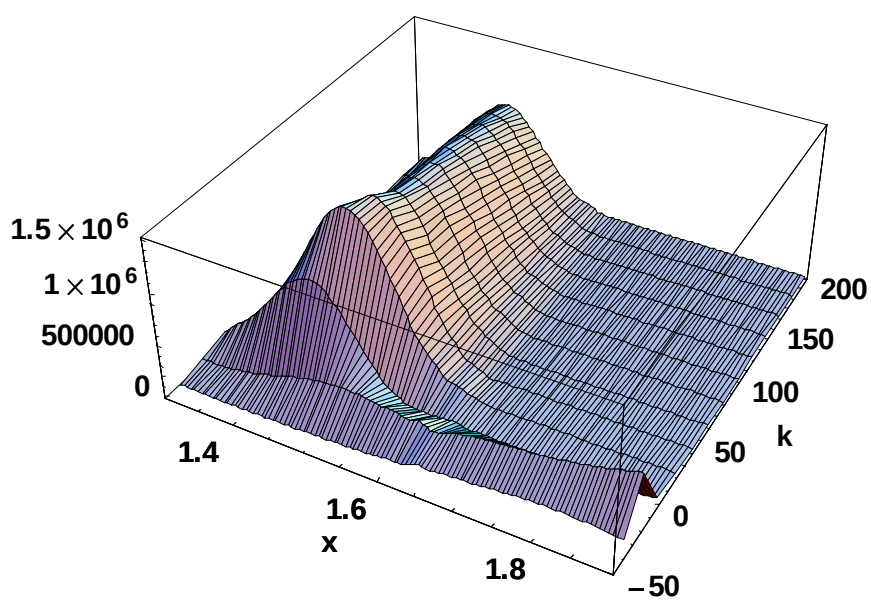

Fig. 1 Spectral power density $P(x_0, k)$ for the Fourier transform of $E_x(x)$ with two window sizes: (a) x_W = 0.25 m, and (b) x_W = 0.05 m.

Test Data for Transform Study

DIII-D D(H) Mode Conversion Reference Case

1D AORSA code run

Case: above the midplane

$E_x(x)$

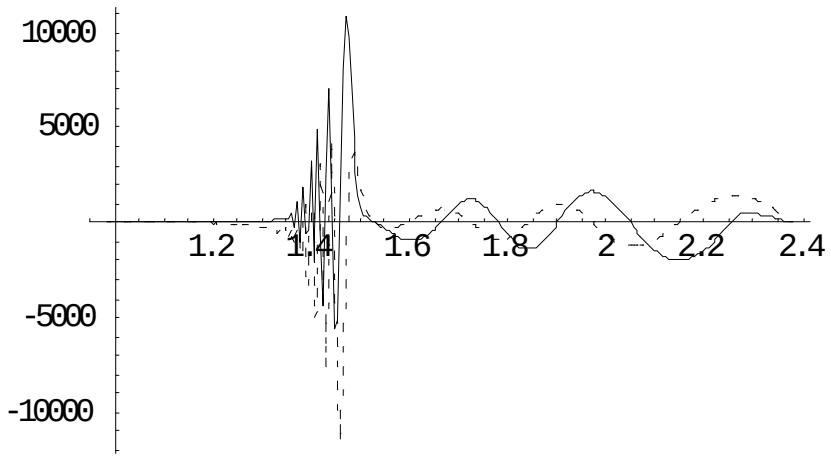

$E_y(x)$

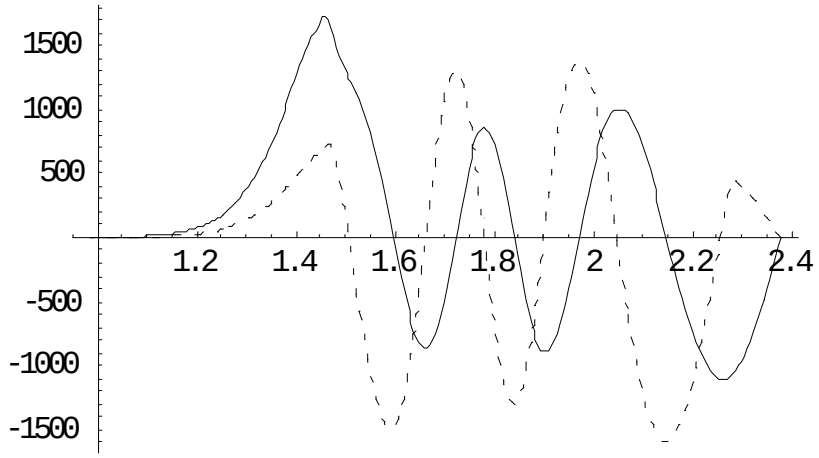

- Test problem used here:

  - o transform $f(x) = E_X(x)$, where $x = R - R_0$. The rf electric field is computed by the 1D AORSA code **[1]** for a DIII-D D(H) mode conversion reference case **[2, 3]**. Units: x(m), k(m^{-1})

  - o The 1D equilibrium includes a model of the 2D *poloidal magnetic field*, which has an important effect on the wave physics ($\Rightarrow$ different above and below the midplane). Unless otherwise stated, the solution used here had parameters corresponding to a horizontal slice of the 2D equilibrium taken *above the midplane*.

See references [Jaeger et al., Phys. Plasmas, 2000 & 2001] and [Batchelor et al., www, 2001] on last poster.

- Fig. 1 shows a 3D plot of the spectral power density $P(x_0, k) = |F(x_0, k)|^2$ for the transform of $E_x(x)$ for two values of x_w:

  - ➢ The *large* window in Fig. 1(a) resolves the incident and reflected FW well, but the mode-converted IBW is not spatially localized.

  - ➢ The *small* window in Fig. 1(b) clearly shows the IBW but the k-structure of the FW is lost.

$\Rightarrow$ A fixed window width (independent of k) can't resolve and localize all k's simultaneously.

Sources of Error & Optimal Windows

The problem with a constant window is that there are two conflicting types of errors: the "Heisenberg" error Δk_1 and the "non-local" or "gradient" error Δk_2, defined as

$$\Delta k_1 = C\frac{\pi}{\Delta x} \quad , \quad \Delta k_2 \approx \frac{\partial k}{\partial x}\Delta x \equiv k'(x)\,\Delta x \quad , \qquad (4)$$

where C = ½ gives good estimates and $\Delta x \approx x_w$. Note that $\Delta k_1(x_w)$ vanishes as $x_w \to \infty$, $\Delta k_2(x_w)$ vanishes as $x_w \to 0$, so the optimal window size is obtained by setting $\Delta k_1(x_w) = \Delta k_2(x_w)$:

$$x_{w,opt} = \left(\frac{\pi}{2k'(x)}\right)^{1/2} \quad . \qquad (5)$$

$\Rightarrow$ the optimal window is a function of k(x)

The Heisenberg formula suggests the scaling $x_w \propto 1/k$, which is naturally implemented using wavelet transforms.

Wavelet Transforms

- Wavelet transforms take the projection of a function f(x) against a family of basis functions obtained by translating and scaling a "mother function". Wavelet basis functions are *spatially-localized*.

- To preserve complex phase information needed to understand wave propagation, we use the "*Morlet wavelet*"

$$\Psi_M\left(\frac{x-x_0}{x_w}\right) = \exp\left[i\,c_0\left(\frac{x-x_0}{x_w}\right)\right]\exp\left[-\frac{(x-x_0)^2}{2\,x_w^{\,2}}\right] \quad , \qquad (6a)$$

with the window scaling

$$x_w = \frac{c_0}{k} \quad . \qquad (6b)$$

- We define the *Morlet wavelet transform* $f(x) \rightarrow W(x_0, k)$ as

$$\begin{aligned} W(x_0,k) &= \frac{1}{N}\sum_{i=1}^{N} f_i\,\Psi^*\left(\frac{x_i-x_0}{x_w}\right) \\ &= \frac{1}{N}\sum_{i=1}^{N} f_i \exp\left[-ic_0\left(\frac{x_i-x_0}{x_w}\right)\right]\exp\left[-\frac{(x_i-x_0)^2}{2\,x_w^{\,2}}\right] \end{aligned} \qquad (7)$$

where the normalization factor 1/N is the same as in the WFT.

Notes:

- The Morlet wavelet transform is equivalent to a Gaussian windowed Fourier transform with x_w scaled to k by Eq. (6b).

- The parameter c_0 controls the ratio Heisenberg / gradient error and has an *optimal value* of about $c_0 = 5$ for our problem. An optimal window exists for a given k when

$$kL_x \;>>\; kx_w = c_0 \;>>\; 1 \quad . \qquad (8)$$

- The number of computations required for the spatial convolution in Eq. (7) scales like **N^2**. The *convolution theorem* can be used to recast this into k-space FFTs, which scales like **N ln N** (much more efficient):

$$W(x_0, k) = \frac{1}{N}\Im^{-1}\left(\Im[f(x)]\,\Im\left[\Psi * \left(\frac{x - x_0}{x_w}\right)\right]\right) , \qquad (9)$$

where $\Im[f(x)]$ denotes the forward Fourier transform of f(x), $\Im^{-1}$ denotes the inverse Fourier transform, and the k dependence on the rhs of Eq. (9) is implicit through Eq. (6b). The wavelet function must be made *periodic* on the x interval.

- The evaluation of FFTs and other necessary manipulations for evaluating these transforms were easily programmed using the built-in functions in *Mathematica*.

Morlet Wavelet Transform Results

- Fig. 2 shows a 3D plot of the spectral power density $P(x_0, k) = |W(x_0, k)|^2$ for the Morlet wavelet transform of $E_x(x)$ given by Eqs. (6b) and (7).

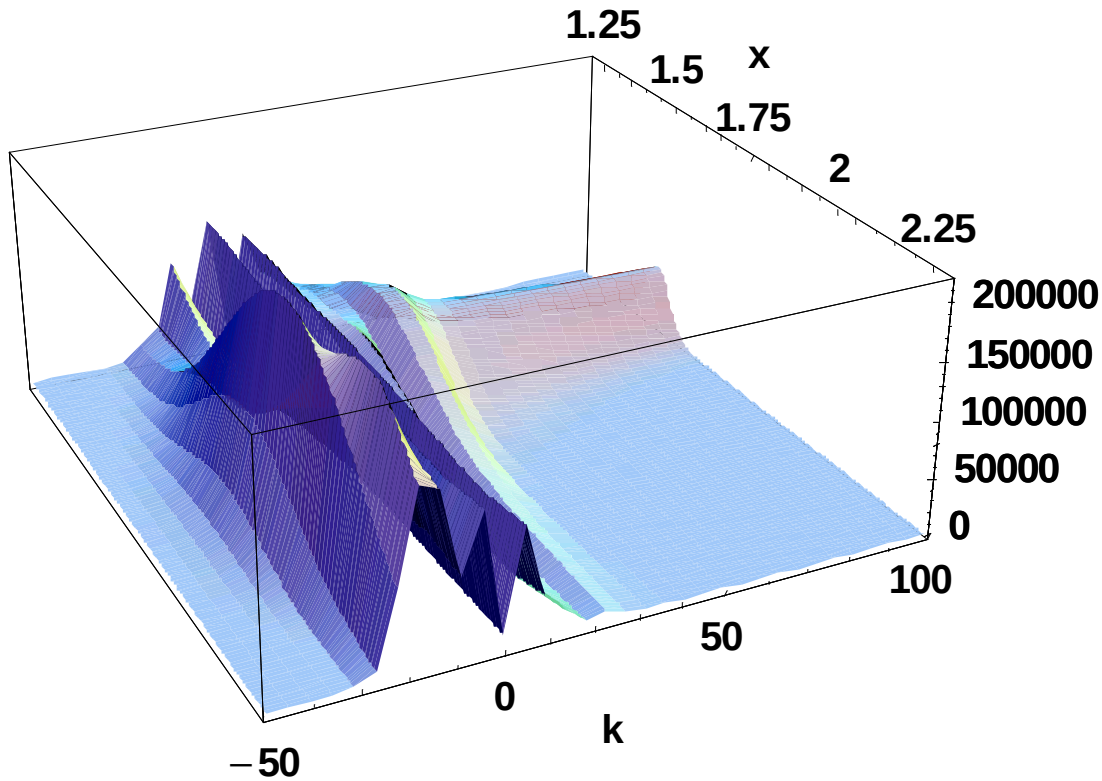

Fig. 2 Spectral power density $P(x_0,k)$ for the Morlet wavelet transform of $E_x(x)$ using the scaling $x_w = c_0/k$ with $c_0 = 6$.

- the Morlet wavelet can resolve both FW and IBW simultaneously
- there are unphysical oscillations near $k = 0$ ($\Rightarrow$ $x_w \to \infty$) due to the gradient error
- we can resolve this singularity by modifying the wavelet function

k-Wavelet Transform

- We have obtained good results with a modified wavelet transform (which we call the "*k-wavelet*") that has the following properties:
  - preserves the scaling (6b) of the Morlet wavelet away from k = 0
  - has a finite window width at k = 0
  - describes windowed plane waves ~ exp[i k x] for all k

- The **k-wavelet** is defined by

$$\Psi[k(x-x_0)] = \exp[i\,k(x-x_0)]\exp\left[-\frac{k^2(x-x_0)^2}{2\,k^2 x_w{}^2}\right] , \quad (10a)$$

$$x_w = \frac{c_0}{\sqrt{k^2 + k_0{}^2}} , \quad (10b)$$

  - k_0 is a parameter that determines the wavelet scale at k = 0: $x_w(k = 0) = c_0/k_0$.
  - not a "pure" wavelet but works well for diagnostic applications.

- Combining Eqs. (9) and (10) gives the wavelet transform $W(x_0, k)$ and the associated spectral power density $P(x_0, k) = |W(x_0, k)|^2$.

k-Wavelet Transform Results

- A 3D plot of the k-wavelet spectral power density (see Fig. 3) shows that all waves are resolved and the behavior at k = 0 is physical:

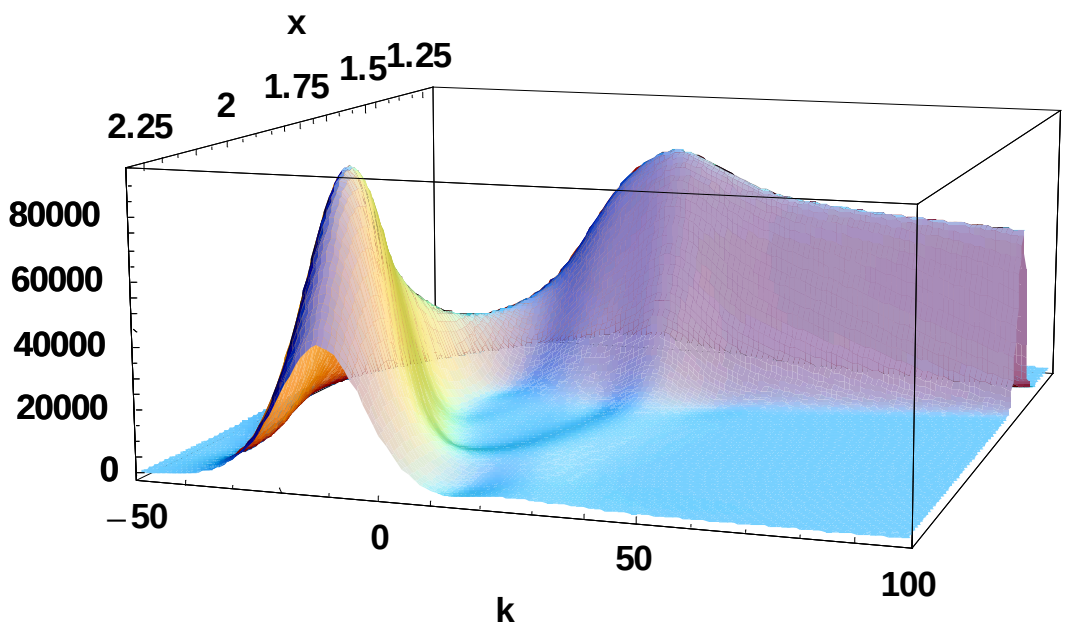

Fig. 3 Spectral power density $P(x_0, k)$ for the k-wavelet transform of $E_x(x)$ using the scaling $x_w = c_0/(k^2 + k_0^2)^{1/2}$ with $c_0 = 5$ and $k_0 = 40\ m^{-1}$.

- Adopt this case as the base case for these posters.

● Contour plots comparing the windowed Fourier transform (WFT) and k-wavelet approaches are shown in Fig. 4. The IBW is much better resolved in the wavelet analysis.

Fig. 4(a) Fig. 4(b)

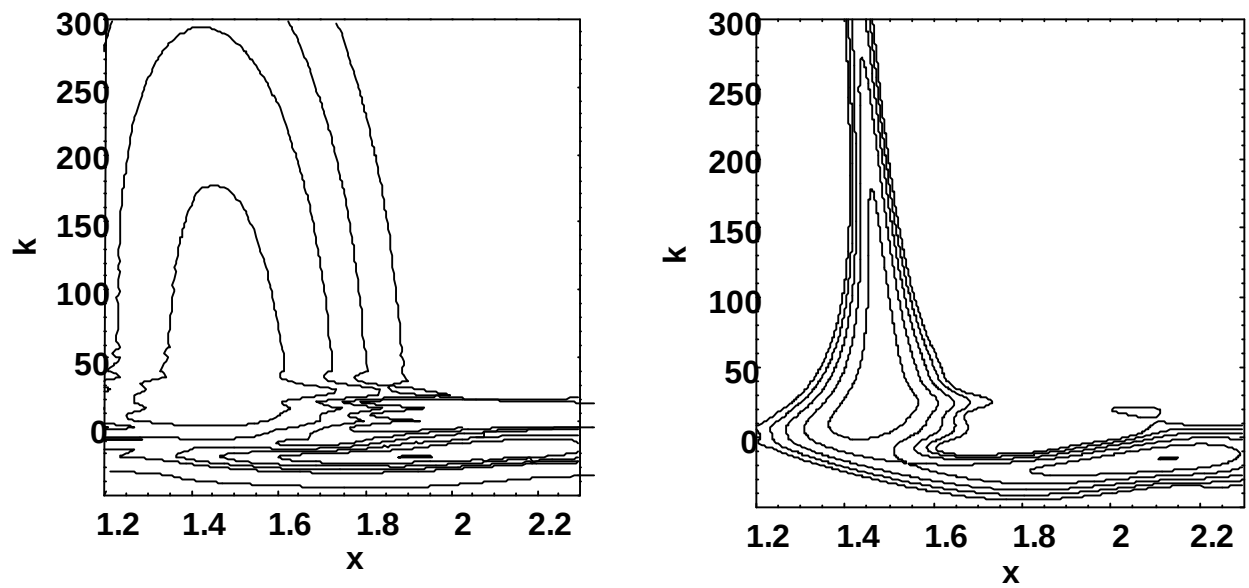

Fig. 4 Contour plots of the spectral power density $P(x_0, k)$ for (a) the windowed Fourier transform of $E_x(x)$ with x_w = 0.25 m, and (b) the k-wavelet transform of $E_x(x)$ using the scaling $x_w = c_0/(k^2 + k_0^2)^{1/2}$ with c_0= 5 and k_0= 40 m^{-1}.

● Note that the wavelet transform provides quantitative information on $k_x = k(x)$:

- the incident FW propagates to the left with k = –25 m^{-1}, the reflected FW propagates to the right with k = +25 m^{-1}.
- k increases for the mode-converted IBW as it propagates into the plasma ⇒ the IBW is a backward propagating wave.

Physics Analysis

1. *Details of FW propagation and reflection*

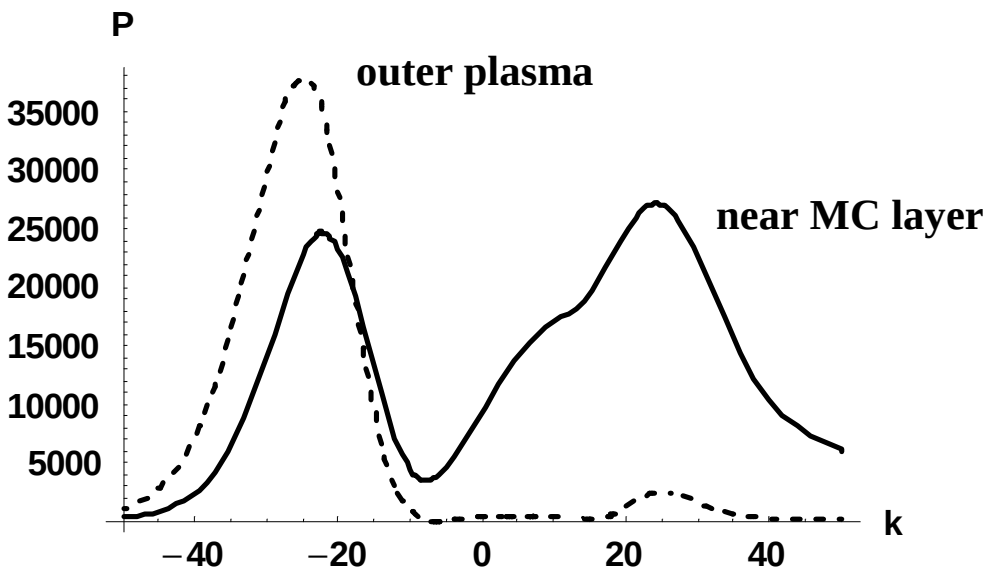

Fig. 5 Plot of the wavelet spectral power density P(k) at fixed x_0 obtained by the k-wavelet transform of $E_x(x)$. The **dashed** curve corresponds to x_0 = 1.75 m, located in the **outer plasma**; the **solid** curve to x_0 = 1.6 m, **near the mode conversion layer**.

- mode conversion surface is near x = 1.5 m
- incident and reflected FW are comparable near x = 1.6 m
- reflected FW negligible for x > 1.75 m

2. *Comparison of 1D rf code results with analytic dispersion relation*

Define $P_\alpha(x_0, k) = |W_\alpha(x_0, k)|^2$, W_α = k-wavelet transform of $E_\alpha(x)$.

$$\Rightarrow \mathbf{P_\perp(x_0, k) = P_x(x_0, k) + P_y(x_0, k)}$$

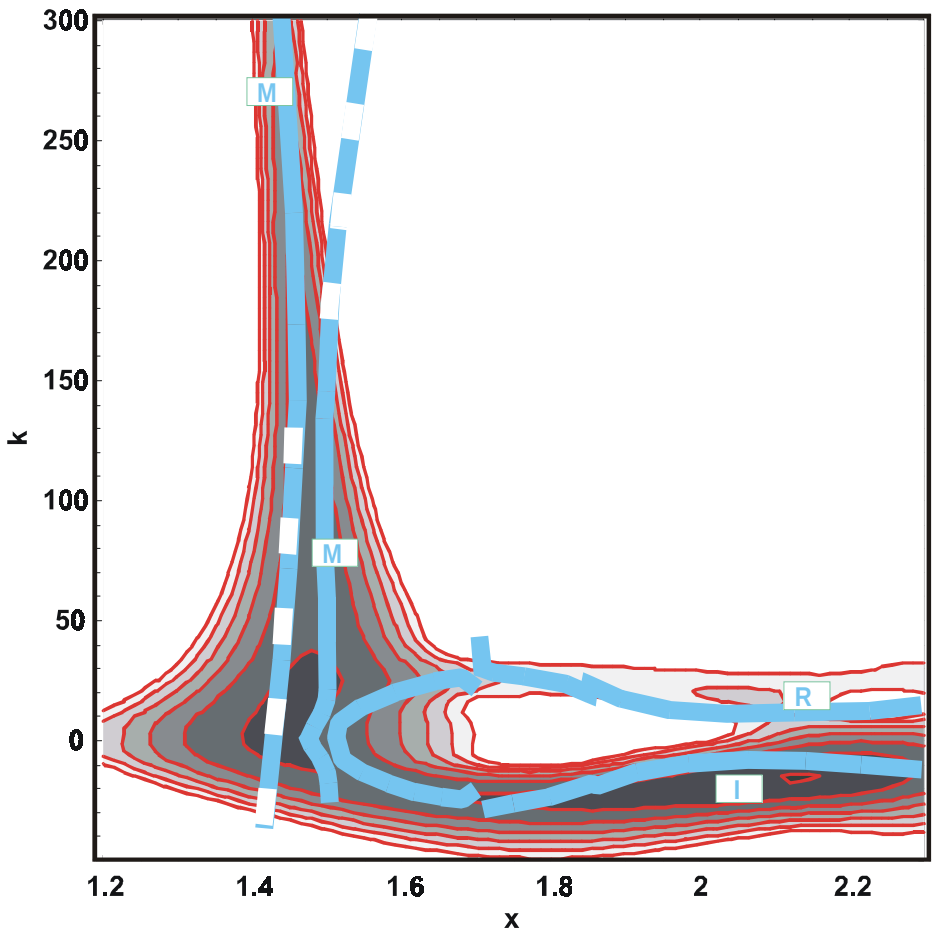

Fig. 6 Comparison of the k-wavelet spectral power density $P_\perp(x_0, k)$ (red contour lines) with the hot-plasma dispersion relation (blue lines). **The solid (dashed) blue lines depict propagating (heavily damped) modes.**

Fig. 6 shows good quantitative agreement between the k-wavelet analysis of the code results and the analytic dispersion relation.

3. Linear wave polarization (E_x/E_y)

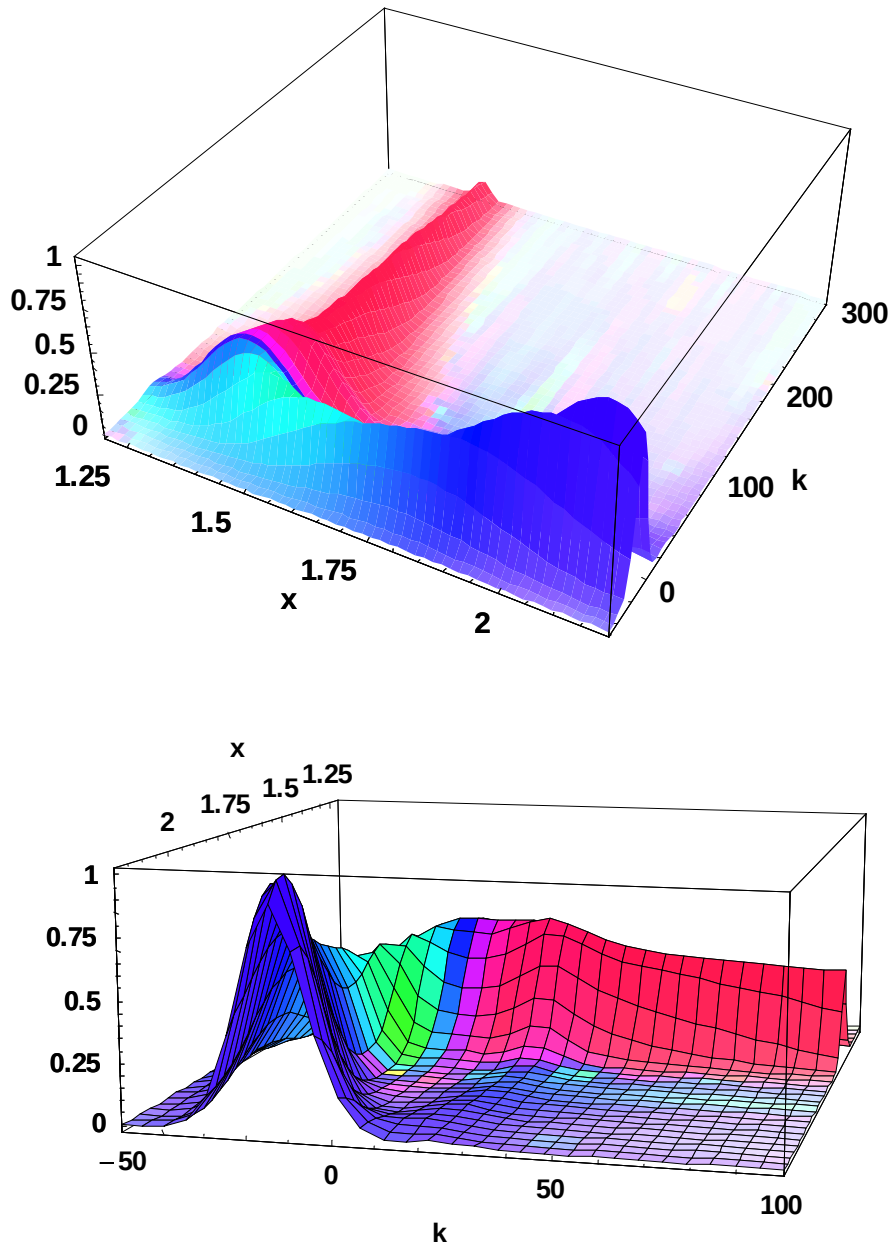

Fig. 7 K-wavelet transform spectral power density $P_\perp(x_0, k)$ of the rf electric field using the same parameters as Fig. 3. Here the color palette indicates the *linear* wave polarization $p = E_x/E_y$; it runs from light green ($p << 1$) through blue ($p \sim 1$) to red ($p >> 1$).

4. Circular wave polarization (E_R/E_L)

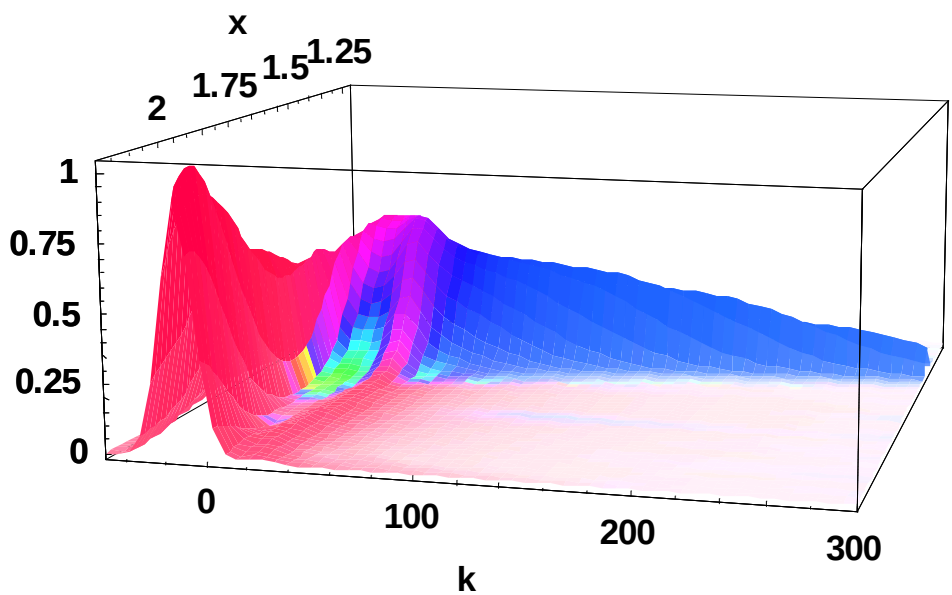

Fig. 8 K-wavelet transform spectral power density $P_\perp(x_0, k)$ of the rf electric field using the same parameters as Fig. 3. Here the color palette indicates the *circular* wave polarization $p = E_R/E_L$; it runs from light green ($p << 1$) through blue ($p \sim 1$) to red ($p >> 1$).

Figs. 7 and 8 illustrate the change of wave polarization from the FW to the IBW and the mixed polarization in the mode-conversion region.

(These figures take advantage of the built-in color functions in *Mathematica*.)

5. Illustrate poloidal B field effect on wave propagation (compare waves above and below midplane, see Fig. 9)

Compare two horizontal cuts:

(a) Above the midplane: backward propagating IBW

(b) Below the midplane: forward propagating ICW

Fig. 9 (a) Fig. 9 (b)

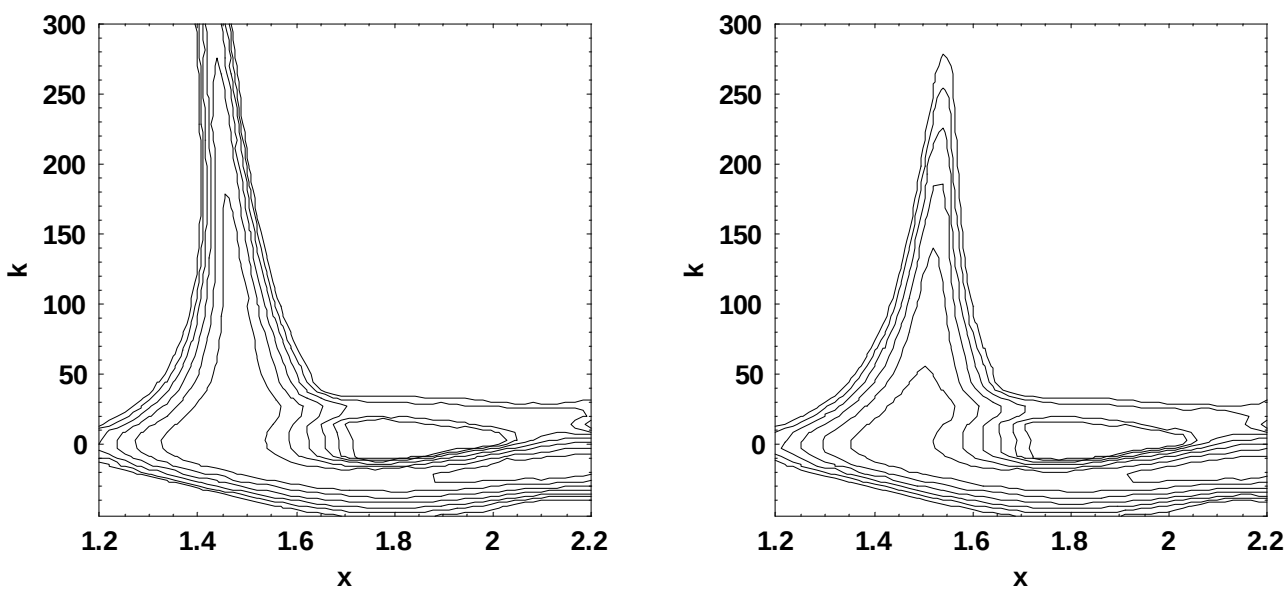

Fig. 9 K-wavelet transform spectral power density $P_{\perp}(x_0, k)$ of the rf electric field for horizontal slices (a) above the midplane, and (b) below the midplane.

Also see posters BP1.074 [Jaeger et al.] and BP1.075 [Berry et al.] and Perkins, Nucl. Fusion, 1977.

Summary & Discussion

● Various Fourier and wavelet transform techniques have been explored for the purpose of visualizing and quantifying wave propagation and dispersion in plasmas.

● The general problem of finding k(x) requires (i) using a localized set of basis functions ("windowed transforms"), and (ii) using an optimal window for each k. Wavelets are well-suited to this problem.

● A modified Morlet wavelet (called here the "k-wavelet") was shown to provide a useful diagnostic for mode conversion scenarios where multiple waves are present with vastly different wavelengths.

● Important physical information (amplitude, polarization, wavenumber, etc.) can be displayed graphically using these transform methods.

● Good agreement was found between the analytic 1D dispersion relation and the numerical results of the 1D full-wave AORSA code.

● This diagnostic was used to illustrate the effect of the poloidal magnetic field on the mode conversion and wave propagation.

● The 1D transform methods used here can be extended to 2D in a straightforward way.

References

AORSA code and mode conversion base case:

E.F. Jaeger, L. A. Berry, and D. B. Batchelor, Phys. Plasmas **7**, 3319 (2000).

E.F. Jaeger, L. A. Berry, E. D'Azevedo, D. B. Batchelor, and M. D. Carter, Phys. Plasmas **8**, 1573 (2001).

D. B. Batchelor, E. F. Jaeger et al., DOE SciDAC project "Numerical Calculations of Wave Plasma Interactions in Multi-dimensional systems," see description and plots for this baseline case at:

http://www.ornl.gov/fed/scidacrf/blc/InitialbaselineEFJ.pdf .

Wavelets:

"Sampling theory and wave propagation," J. Morlet, NATO ASI, Vol. F1, *Issues on Acoustic Signal/Image Processing and Recognition*, ed. C. H. Chen (Springer, Berlin, 1983); "Decomposition of Hardy functions into square integrable wavelets of constant shape," A. Grossmann and J. Morlet, SIAM J. Math. **15**, 723 (1984).

"Wavelet transforms and their applications to turbulence," M. Farge, Annu. Rev. Fluid Mech. **24**, 395 (1992).

"An Introduction to Wavelets," A. Graps, IEEE Computational Science and Engineering, vol. 2, (1995); also available at

http://www.amara.com/IEEEwave/IEEEwavelet.html .

"Wavelets for kids – A Tutorial Introduction," B. Vidakovic and P. Mueller, December, 1994; available at

http://www.isye.gatech.edu/~brani/wp/kidsA.pdf .

"A Practical Guide to Wavelet Analysis," C. Torrence and G. Compo, Bulletin of the American Meteorological Society **79**, 61 (1998).